Electronic Supplementary Information

Chiral Resolution of Racemic Ibuprofen Sodium via Diastereomeric Ionic Cocrystallization with Proline

Ting Wen,[a] Koen Robeyns,[a] Laurent Collard,[a] Tom Leyssens,[a *] and Fucheng Leng [b *]

[a] Institute of Condensed Matter and Nanosciences, Université catholique de Louvain, Place Louis Pasteur 1, 1348 Louvain-La-Neuve, Belgium

[b] Food Science Building, University College Cork, College Road, Ireland

1. Experimental

1.1 Materials

Racemic ibuprofen (RS-Ibu) was bought from Angene Chemical. Racemic sodium ibuprofen dihydrate (RS-IbuNa·2H_2O) was purchased from Merck. S-ibuprofen was bought from Angene Chemical, and further converted to its corresponding sodium salt form (S-IbuNa·2H_2O) through reaction with NaOH obtained from Fisher Scientific. D-proline (D-pro) was bought from Apollo Scientific. L-proline (L-pro) was obtained from Fisher Scientific. Hexane (Hex), isopropanol (IPA) and additional solvents were bought from VWR and employed as obtained without further processing.

1.2 Characterization

Powder X-ray Diffraction (PXRD)

PXRD data were collected on a Bruker D8 diffractometer with Cu Kα radiation source (λ = 1.5406 Å). The experiments were performed at 40 kV and 30 mA, scanning the 2θ range from 4° to 40° with a step size of 0.02°.

Variable Temperature Powder X-ray Diffraction (VT-PXRD).

A Bruker D8 Discover X-ray diffractometer, configured with a Cu Kα source (λ = 1.5406 Å) and operated at 40 kV and 30 mA, was employed to monitor the phase transitions and dehydration behavior of the ionic cocrystals. The diffraction data were recorded over a 2θ range of 4-40° with a 0.015° step size, while the temperature was ramped from 25 °C to 105 °C in 10 °C increments.

Single crystal X-ray Diffraction (SCXRD)

Diffraction data were collected utilizing an Incoatec IμS microfocus source (Mo Kα, λ = 0.71073 Å) coupled with a MAR345 image plate detector. Following data collection, all data were integrated and reduced using CrysAlis^{PRO}.[1] The crystal structures were solved via the dual-space method intrinsic to SHELXT[2] and were subsequently refined against F^2 with SHELXL[3].

Differential Scanning Calorimetry (DSC)

Thermal properties of the ionic cocrystals were analysed using a TA Instruments DSC2500 calibrated with indium. Following the preparation of samples (5-8 mg) in sealed aluminium Tzero pans, the data were acquired over a temperature range of 25 to 220 °C. The samples were heated at 10 °C/min under a constant nitrogen flow of 50 mL/min.

Thermogravimetric Analysis (TGA)

TGA analyses were carried out on a Mettler Toledo TGA/DSC 3+ instrument, where samples (5-10 mg) in open aluminum oxide crucibles were heated from 25 to 300 °C at 10 °C/min under a continuous nitrogen purge.

Dynamic Vapor Sorption (DVS)

A TA Q5000 analyser was employed for DVS measurement. Approximately 5 mg of the samples was weighed into a quartz pan, and then exposed to the following RH levels: 30-80% in 5% increments at 25 °C. The system proceeded to the next RH level after the sample reached equilibrium, which was defined as a mass change of less than 0.01% for 10 min (maximum dwell time 360 min).

Chiral High-Performance Liquid Chromatography (cHPLC)

Chiral HPLC analyses were carried out using a Waters Alliance 2690 separation module coupled to a Waters 2998 photodiode array (PDA) detector. Samples were diluted in acetonitrile/water (50:50, v/v) prior to injection, and 10 µL were injected for each analysis. Chromatographic separation was achieved on a Phenomenex Lux Amylose-1 chiral stationary phase (250 × 4.6 mm, 5 µm particle size). The mobile phase consisted of acetonitrile and water (50:50, v/v) supplemented with 0.1% formic acid and was delivered under isocratic conditions at a flow rate of 1.0 $mL \cdot min^{-1}$. All separations were performed at ambient temperature. Detection was accomplished using the PDA detector with UV extraction at 220 nm. The total run time was 15 min. Data acquisition and processing were performed using Empower 2 chromatography software (Waters). Under these conditions, baseline separation of the enantiomers was achieved, with retention times of 7.4 min for the first-eluting enantiomer and 8.2 min for the second-eluting enantiomer. Enantiomeric excess (ee) values were determined from the integrated peak areas of the two enantiomers.

1.3 Sample preparation

1.3.1 ionic cocrystals screening

The liquid-assisted grinding (LAG) method was employed to screen for the formation of diastereomeric cocrystals. An equimolar mixture of 0.5 mmol RS-Ibu or RS-IbuNa·$2H_2O$ and the corresponding amino acids was added to an Eppendorf tube, together with 10 μL of EtOH and three stainless steel balls (3 mm in diameter). The mixture was then subjected to grinding using a RETSCH Mixer Mill MM 400 at 30 Hz for 50 minutes. The PXRD patterns of the resulting powders were subsequently compared with starting materials to detect the occurrence of any new diffraction peaks.

1.3.2 Single crystal growth

Single crystals of S-D·$2H_2O$ and S-L were obtained from a mixed solvent of IPA/Hex (30:70, v/v). An equimolar mixture of RS-IbuNa·$2H_2O$ and D-pro was ground, and approximately 10 mg of the resulting powder was dissolved in 3 mL of solvent. The solution was slowly evaporated at room temperature to obtain S-D·$2H_2O$ crystals. The S-L single crystal was obtained following the procedure described above, but using S-IbuNa·$2H_2O$ and L-pro.

1.3.3 Synthesis of S-D·$2H_2O$ and S-L

Theoretically, the diastereomeric cocrystal pair formed by RS-IbuNa·$2H_2O$ and D-pro are S-D·$2H_2O$ and R-D·$2H_2O$. However, R-D and S-L are enantiomerically related, with identical scalar properties. Therefore, S-L was used as a substitute for R-D throughout the experiments. In addition, S-L (R-D) is always obtained in anhydrous form. Both LAG and slurry methods can be employed to synthesize two ionic cocrystals. The procedure of LAG method is identical to that used in the screening experiments, except that S-IbuNa·$2H_2O$ was used. Slurry experiments were performed using an equimolar mixture of the starting materials in a mixed solvent of IPA/Hex (10:90, v/v), and these slurries were stirred at room temperature for 48 h. All ionic cocrystal powders used for subsequent thermal characterization were obtained via the slurry method.

1.3.4 Solvents screening

Several solvents were screened by slurry experiments. In a typical experiment, 150 mg of RS-IbuNa·2H_2O and 65.34 mg of D-pro were suspended in 1 mL of different solvents and stirred at room temperature for 48 h. The resulting slurries were filtrated using a funnel to collect the powder for PXRD analysis.

1.3.5 Construction of the isoplethal ternary phase diagram

The isoplethal ternary phase diagram was constructed by suspending RS-IbuNa·2H_2O and D-pro at different molar ratios (0 to 1) in different amounts of solvent. Each experiment was performed in a sealed 4 mL vial, and the suspensions were continuously stirred at 25 °C for 48 h. Seeds of all possible solid forms were added into the suspensions. After equilibration, the mixtures were filtered, and the obtained solid phases were analyzed by PXRD.

1.3.6 Chiral resolution experiments

The chiral resolution process was performed by slurry crystallization using 150 mg RS-IbuNa·2H_2O and 65.34 mg D-pro (1:1), with solvent volumes of 1.2, 1.6, 2.0, 2.4, and 2.8 mL of IPA /Hex (10:90, v/v). The procedure was the same as previously described, except that an additional washing step was included. The filtered solid phases were washed with the same solvent used in the slurry crystallization to remove residual mother liquor. After drying at 40 °C, the *ee* value was determined by cHPLC.

1.3.6 Scale-up experiment

1.5 g of RS-IbuNa·2H_2O and 0.653 g of D-pro (1:1) were dissolved in 3 mL of IPA in a 50 mL Erlenmeyer flask, after which 27 mL of hexane was added. The flask was sealed and stirred for 48 h. The resulting powder was then filtered, dried, and characterized by PXRD and cHPLC.

1.3.7 Dissociation of ionic cocrystal

The 100 mg powder obtained from the upscaled experiment was suspended in 1 mL of a 0.075 g/mL NaCl solution, stirred for 5 h, and then filtered. The resulting solid was analyzed by PXRD and cHPLC.

2. Results

RS-Ibu was subjected to diastereomeric cocrystal screening with ten amino acids via LAG approach. (**Table S1**). The cocrystal formed with L-pro was identified as a solid solution. This conclusion was supported by PXRD analysis of RS-Ibu-L-pro (1:1) and RS-Ibu/S-Ibu mixtures with L-pro prepared by LAG method, as well as by comparison of the PXRD patterns of the solid phase obtained from the RS-Ibu/L-pro (1:1) slurry in hexane with the reported pattern of S-Ibu-L-pro·0.25H_2O, together with cHPLC analysis.[4] The detailed results are shown in **Fig. S1** and **Fig. S2**.

Table S1. Screening Results for RS-Ibu

Amino acids	RS-Ibu	Amino acids	RS-Ibu
D-Threonine	×	L-Phenylalanine	×
D-Tryptophan	×	L-/D-Proline	√
D-Tyrosine	×	L-Isoleucine	×
L-Serine	×	L-Lysine	√
D-Leucine	×	D-Methionine	×

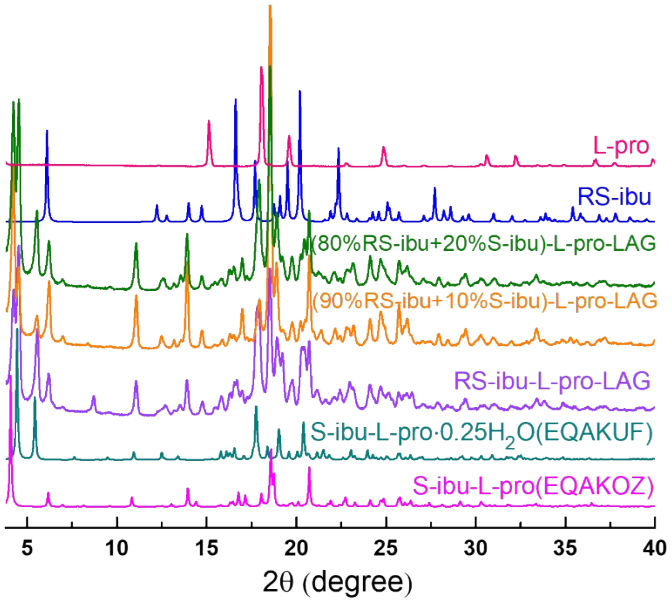

Fig. S1 PXRD patterns of RS-Ibu+L-pro (1:1) and RS-Ibu/S-Ibu mixtures with L-pro by LAG.

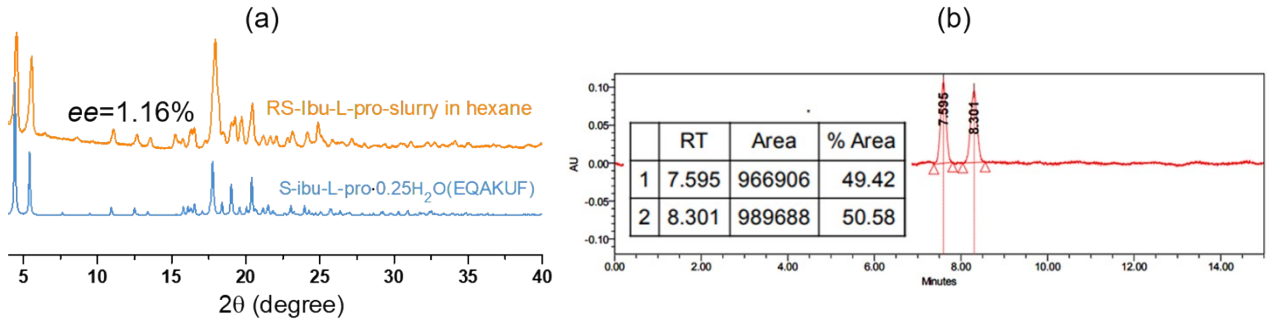

Fig. S2 Solid phase collected from hexane: (a) PXRD pattern compared with S-Ibu-L-pro·0.25H_2O; (b)chiral HPLC result.

Table S2. Screening results for RS-IbuNa·2H_2O

Amino acids	RS-IbuNa·2H_2O	Amino acids	RS-IbuNa·2H_2O
D-Threonine	×	L-Phenylalanine	×
D-Tryptophan	×	L-/D-Proline	√
D-Tyrosine	×	L-Isoleucine	×
L-Serine	×	L-Lysine	×
D-Leucine	×	D-Methionine	×

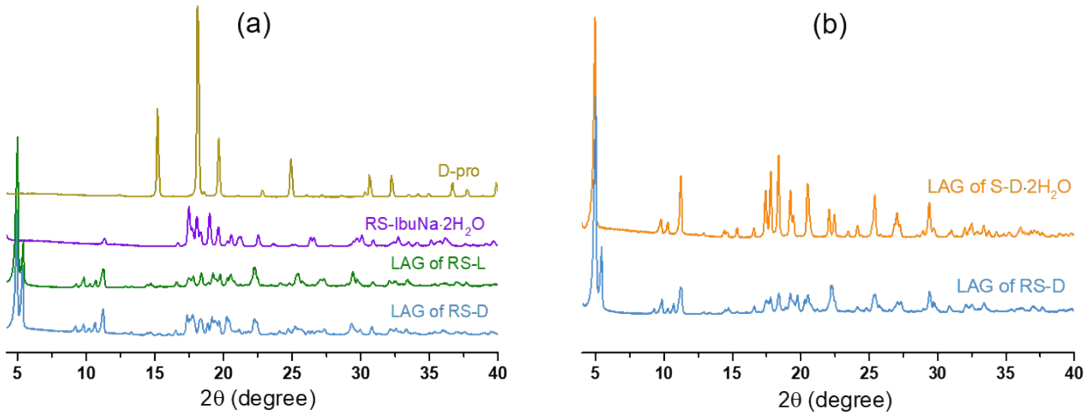

Fig. S3 Experimental PXRD patterns: (a) RS-D; (b) the comparison of RS-D and S-D·2H_2O.

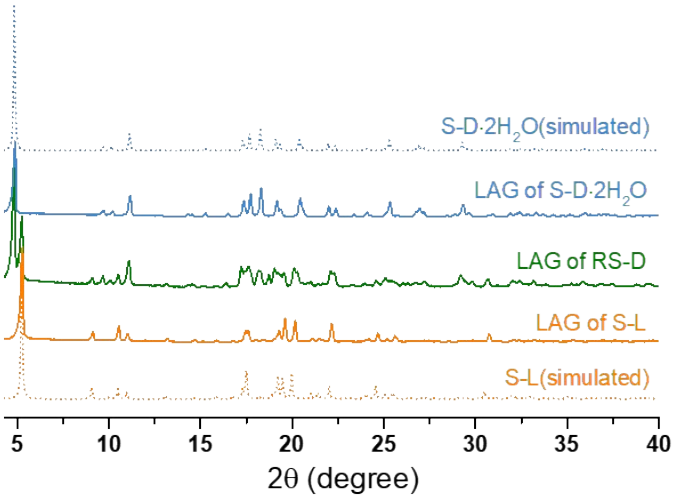

Fig. S4 Simulated (dash lines) and experimental (solid lines) PXRD patterns of S-D·2H₂O and S-L.

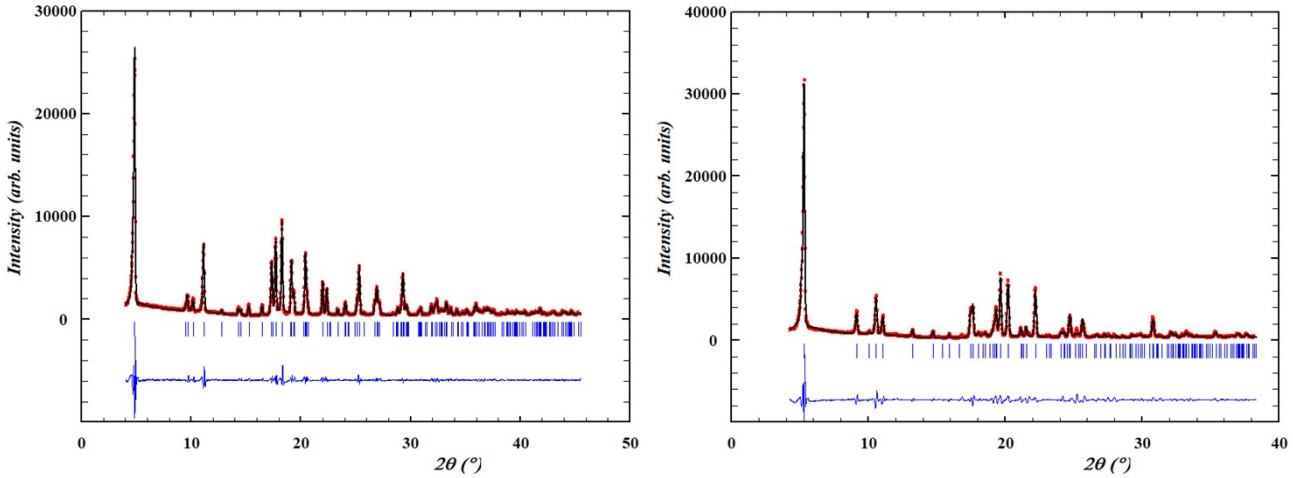

Fig. S5 Profile fitting of experimental S-D·2H₂O (left) and S-L (right) PXRD patterns (red, experimental pattern; black, calculated pattern; blue, difference curve; vertical blue bars indicate peak positions).

Table S3. Crystallographic data of S-D·2H_2O and S-L

Compound	S-D·2H_2O	S-L
CCDC number	2530249	2530250
Formula	$C_{18}H_{30}NO_6Na$	$C_{18}H_{26}NO_4Na$
Formula weight (g·mol^{-1})	379.42	343.39
Temperature/K	297(2)	297(2)
Crystal system	monoclinic	triclinic
Space group	$P2_1$	$P1$
a (Å)	9.3842(6)	5.7825(6)
b (Å)	6.1358(5)	9.8484(10)
c (Å)	18.3975(17)	17.0500(15)
α (°)	90	83.265(8)
β (°)	96.437(7)	84.387(8)
γ (°)	90	85.997(8)
Volume (Å^3)	1052.65(15)	957.97(16)
Z	2	2
ρ_{cal} (g·cm^{-3})	1.197	1.190
Crystal size (mm^3)	0.5 × 0.45 × 0.03	0.5 × 0.1 × 0.06
Radiation(Å)	MoKα (λ = 0.71073)	MoKα (λ = 0.71073)
Reflections collected	10131	6539
Independent reflections	4227	6539
R_{int}	0.0378	0.046[#]
Compl. to θ = 25.242° (%)	98.7	99.7
Data / restraints / parameters	4227 / 225 / 341	6539 / 295 / 618
Goodness-of-fit on F^2	1.082	1.046
Final R indexes [I>=2σ (I)]	R_1 = 0.0545, wR_2 = 0.1538	R_1 = 0.0517, wR_2 = 0.1249
Final R indexes [all data]	R_1 = 0.0597, wR_2 = 0.1570	R_1 = 0.0652, wR_2 = 0.1356
Flack parameter[£]	0.26(19)	0.4(3)
Dr (max, min) (e.Å^{-3})	0.250, -0.249	0.249, -0.201

[#] The S-L crystal was identified as a twin (2-fold rotation around [1 0 0], identified by the twinrotmat method in PLATON), and refined against HKLF 5 formatted data, R_{int} of the HKLF4 data is reported, refining against HKLF5 formatted data imposes Merge 0.

[£] Absolute structure was determined relative to the enantiomeric pure proline.

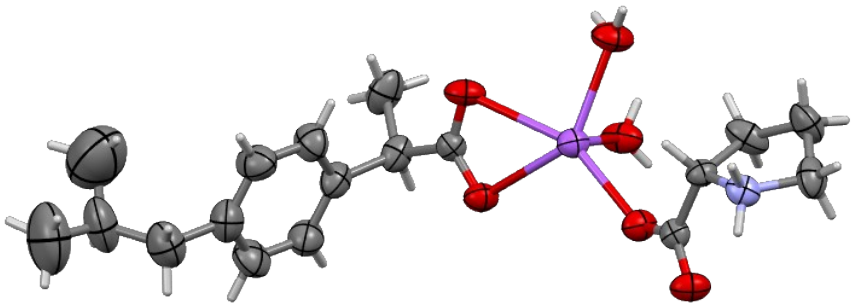

Fig. S6 ORTEP representation of S-D·2H_2O with displacement ellipsoids drawn at the 50% probability level. Carbon atoms are depicted in grey, oxygen atoms in red, sodium atoms in purple. Hydrogen atoms are shown as capped sticks for clarity.

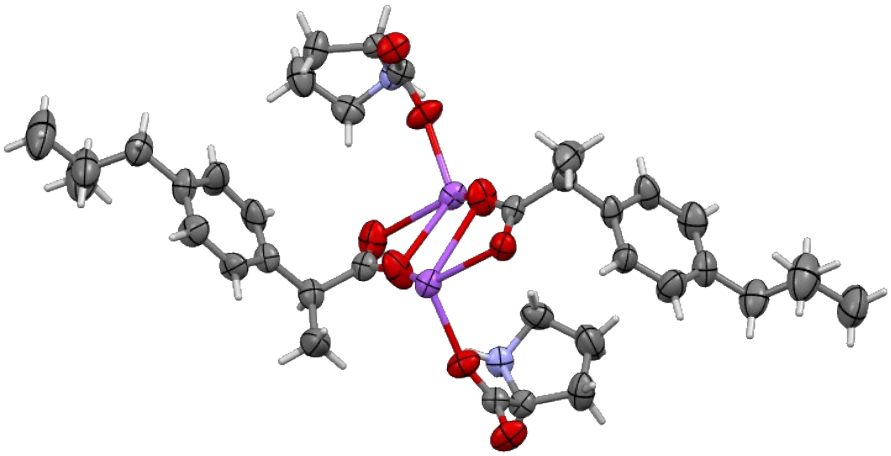

Fig. S7 ORTEP representation of S-L with displacement ellipsoids drawn at the 50% probability level. Carbon atoms are depicted in grey, oxygen atoms in red, sodium atoms in purple. Hydrogen atoms are shown as capped sticks for clarity.

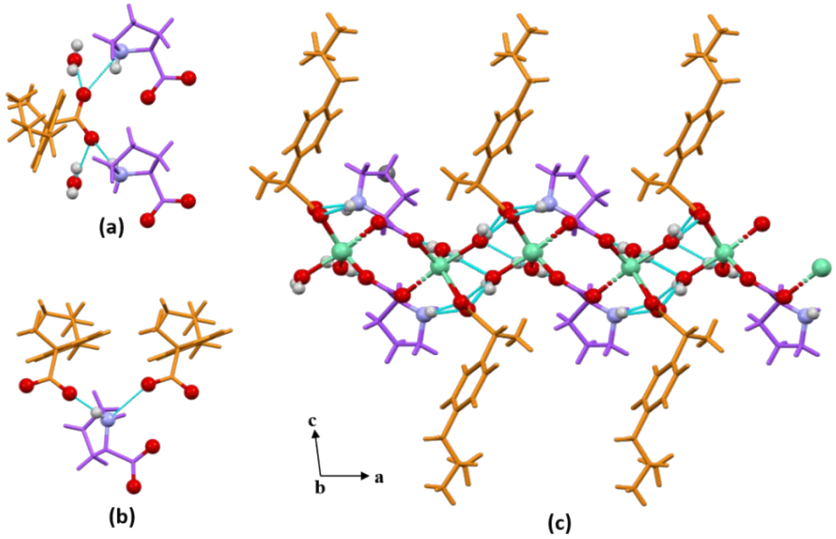

Fig. S8 Hydrogen bonding (cyan dash lines) in S-D·2H_2O between S-ibuprofenates (yellow) and D-pro zwitterions (purple): (a) around S-ibuprofenates; (b) around D-pro zwitterions; (c) in crystal packing.

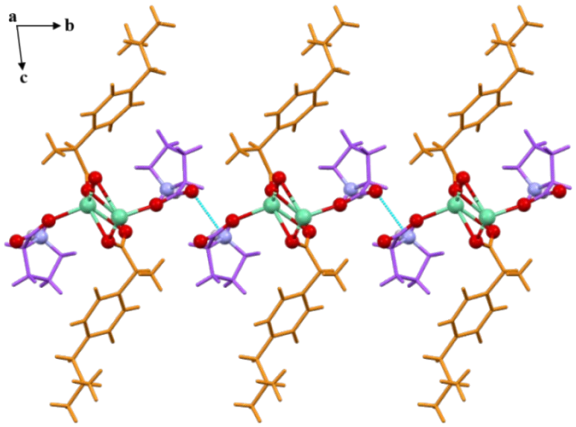

Fig. S9 Hydrogen bonding (cyan dash lines) in S-L between S-ibuprofenates (yellow) and D-pro zwitterions (purple): (a) around S-ibuprofenates; (b) around D-pro zwitterions; (c) in crystal packing.

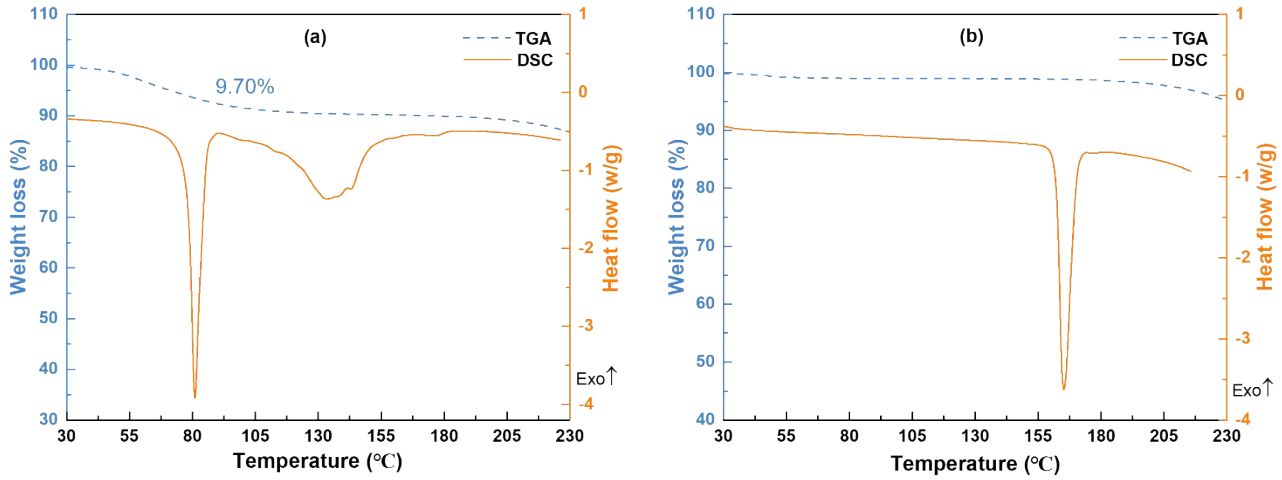

Fig. S10 DSC and TGA curves: (a)S-D·2H_2O; (b)S-L.

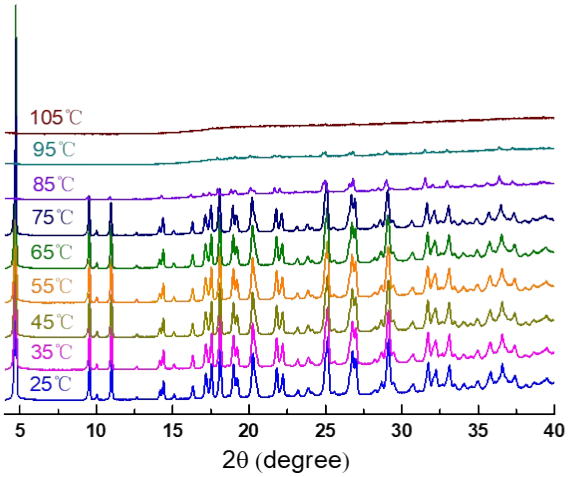

Fig. S11 VT-PXRD of S-D·2H_2O.

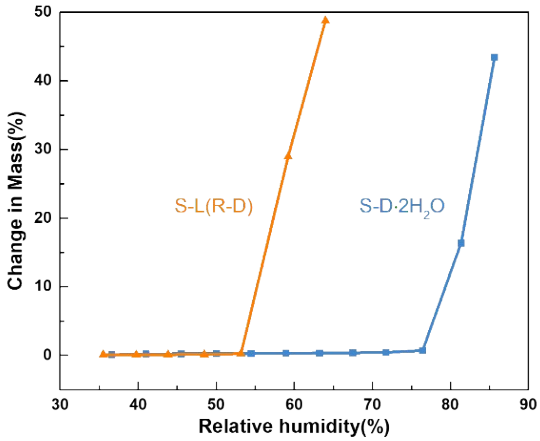

Fig. S12 DVS curves of S-D·2H_2O and S-L.

Table S4. Outcome of solvent screening experiments

Solvent	Outcome	Solvent	Outcome
MeOH	too soluble	EtOAc	×
EtOH	too soluble	Hexane (Hex)	×
IPA	too soluble	MeOH/ACN (10:90, v/v)	×
butanol	too soluble	IPA/ACN (10:90, v/v)	×
acetone	sticky	IPA/Hex (10:90, v/v)	S-D·2H_2O+R-D
ACN	sticky	acetone/Hex (10:90, v/v)	sticky
diethyl ether	sticky	diethyl ether/Hex (10:90, v/v)	sticky
H_2O	too soluble	THF/Hex (10:90, v/v)	sticky
Toluene	×	-	-

Table S5-1. Solid phases obtained from different ratios of RS-IbuNa·2H_2O:D-pro:IPA/Hex (10:90, v/v) following equilibration at 25 °C

Initial Composition RS-IbuNa·2H_2O:D-pro (mol%)	RS-IbuNa·2H_2O (mg)	D-pro (mg)	Solvent (µL)	RS-IbuNa·2H_2O (mol%)	D-pro (mol%)	Solvent (mol%)	Solid phase at equilibrium
90:10	47.69	2.31	300	6.82	0.76	92.42	S-D·2H_2O + RS-IbuNa·2H_2O
80:20	45.09	4.91	300	6.42	1.60	91.98	S-D·2H_2O + R-D + RS-IbuNa·2H_2O
70:30	42.13	7.87	300	5.97	2.56	91.48	S-D·2H_2O + R-D + RS-IbuNa·2H_2O
60:40	38.75	11.25	300	5.45	3.64	90.91	S-D·2H_2O + R-D + RS-IbuNa·2H_2O
50:50	34.83	15.17	300	4.87	4.87	90.27	S-D·2H_2O + R-D
40:60	30.24	19.76	300	4.19	6.29	89.52	S-D·2H_2O + R-D + D-pro
30:70	24.79	25.21	300	3.40	7.94	88.66	S-D·2H_2O + R-D + D-pro
20:80	18.23	31.77	300	2.47	9.89	87.63	S-D·2H_2O + R-D + D-pro
10:90	10.16	39.84	300	1.36	12.23	86.41	S-D·2H_2O + D-pro

Table S5-2. Solid phases obtained from different ratios of RS-IbuNa·2H_2O:D-pro:IPA/Hex (10:90, v/v) following equilibration at 25 °C

Initial Composition RS-IbuNa·2H_2O:D-pro (mol%)	RS-IbuNa·2H_2O (mg)	D-pro (mg)	Solvent (µL)	RS-IbuNa·2H_2O (mol%)	D-pro (mol%)	Solvent (mol%)	Solid phase at equilibrium
90:10	47.69	2.31	500	4.22	0.47	95.31	S-D·2H_2O + RS-IbuNa·2H_2O
80:20	45.09	4.91	500	3.98	0.99	95.03	S-D·2H_2O + R-D + RS-IbuNa·2H_2O
70:30	42.13	7.87	500	3.71	1.59	94.71	S-D·2H_2O + R-D + RS-IbuNa·2H_2O
60:40	38.75	11.25	500	3.39	2.26	94.34	S-D·2H_2O + R-D + RS-IbuNa·2H_2O
50:50	34.83	15.17	500	3.04	3.04	93.92	S-D·2H_2O + R-D
40:60	30.24	19.76	500	2.62	3.94	93.44	S-D·2H_2O + R-D + D-pro
30:70	24.79	25.21	500	2.14	4.99	92.87	S-D·2H_2O + R-D + D-pro
20:80	18.23	31.77	500	1.56	6.24	92.19	S-D·2H_2O + R-D + D-pro
10:90	10.16	39.84	500	0.86	7.76	91.38	S-D·2H_2O + D-pro

Table S5-3. Solid phases obtained from different ratios of RS-IbuNa·$2H_2O$:D-pro:IPA/Hex (10:90, v/v) following equilibration at 25 °C

Initial Composition RS-IbuNa·$2H_2O$:D-pro (mol%)	RS-IbuNa·$2H_2O$ (mg)	D-pro (mg)	Solvent (µL)	RS-IbuNa·$2H_2O$ (mol%)	D-pro (mol%)	Solvent (mol%)	Solid phase at equilibrium
90:10	47.69	2.31	1000	2.16	0.24	97.60	RS-IbuNa·$2H_2O$
80:20	45.09	4.91	1000	2.04	0.51	97.45	S-D·$2H_2O$ + RS-IbuNa·$2H_2O$
70:30	42.13	7.87	1000	1.90	0.82	97.28	S-D·$2H_2O$ + RS-IbuNa·$2H_2O$
60:40	38.75	11.25	1000	1.75	1.16	97.09	S-D·$2H_2O$ + R-D + RS-IbuNa·$2H_2O$
50:50	34.83	15.17	1000	1.57	1.57	96.87	S-D·$2H_2O$ + R-D
40:60	30.24	19.76	1000	1.36	2.04	96.61	S-D·$2H_2O$ + R-D + D-pro
30:70	24.79	25.21	1000	1.11	2.59	96.30	S-D·$2H_2O$ + R-D + D-pro
20:80	18.23	31.77	1000	0.81	3.25	95.94	S-D·$2H_2O$ + D-pro
10:90	10.16	39.84	1000	0.45	4.06	95.49	D-pro

Table S5-4. Solid phases obtained from different ratios of RS-IbuNa·$2H_2O$:D-pro:IPA/Hex (10:90, v/v) following equilibration at 25 °C

Initial Composition RS-IbuNa·$2H_2O$:D-pro (mol%)	RS-IbuNa·$2H_2O$ (mg)	D-pro (mg)	Solvent (µL)	RS-IbuNa·$2H_2O$ (mol%)	D-pro (mol%)	Solvent (mol%)	Solid phase at equilibrium
90:10	47.69	2.31	2000	1.09	0.12	98.79	RS-IbuNa·$2H_2O$
80:20	45.09	4.91	2000	1.03	0.26	98.71	RS-IbuNa·$2H_2O$
70:30	42.13	7.87	2000	0.96	0.41	98.62	S-D·$2H_2O$ + RS-IbuNa·$2H_2O$
60:40	38.75	11.25	2000	0.89	0.59	98.52	S-D·$2H_2O$ + RS-IbuNa·$2H_2O$
50:50	34.83	15.17	2000	0.79	0.79	98.41	S-D·$2H_2O$
40:60	30.24	19.76	2000	0.69	1.03	98.28	S-D·$2H_2O$ + D-pro
30:70	24.79	25.21	2000	0.56	1.32	98.12	D-pro
20:80	18.23	31.77	2000	0.41	1.66	97.93	D-pro
10:90	10.16	39.84	2000	0.23	2.07	97.70	D-pro

Table S5-5. Solid phases obtained from different ratios of RS-IbuNa·$2H_2O$:D-pro:IPA/Hex (10:90, v/v) following equilibration at 25 °C

Initial Composition RS-IbuNa·$2H_2O$:D-pro (mol%)	RS-IbuNa·$2H_2O$ (mg)	D-pro (mg)	Solvent (µL)	RS-IbuNa·$2H_2O$ (mol%)	D-pro (mol%)	Solvent (mol%)	Solid phase at equilibrium
90:10	47.69	2.31	3500	0.63	0.07	99.30	RS-IbuNa·$2H_2O$
80:20	45.09	4.91	3500	0.59	0.15	99.26	RS-IbuNa·$2H_2O$
70:30	42.13	7.87	3500	0.55	0.24	99.21	RS-IbuNa·$2H_2O$
60:40	38.75	11.25	3500	0.51	0.34	99.15	Too little powder
50:50	34.83	15.17	3500	0.46	0.46	99.09	dissolved
40:60	30.24	19.76	3500	0.40	0.60	99.01	D-pro
30:70	24.79	25.21	3500	0.33	0.76	98.92	D-pro
20:80	18.23	31.77	3500	0.24	0.95	98.81	D-pro
10:90	10.16	39.84	3500	0.13	1.20	98.67	D-pro

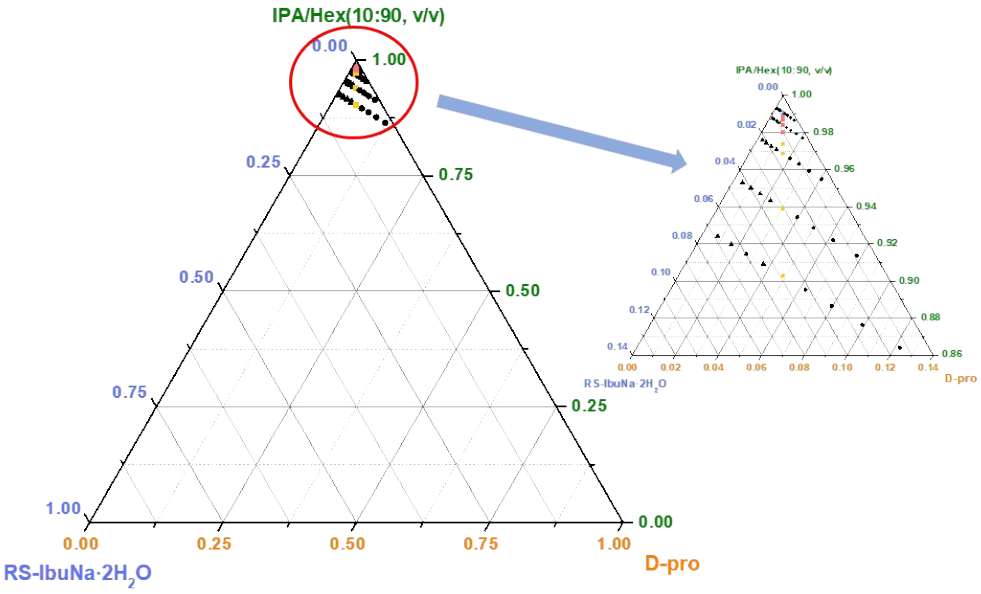

Fig. S13 The full isoplethal ternary phase diagram (mole fraction) between RS-IbuNa·2H_2O, D-pro and IPA/Hex (10:90, v/v).

Table S6. Solid phases obtained from five chiral resolution experiments

Composition RS-IbuNa·2H_2O: D-pro (mol%)	RS-IbuNa·2H_2O (mg)	D-pro (mg)	Solvent (μL)	RS-IbuNa·2H_2O (mol%)	D-pro (mol%)	Solvent (mol%)	Solid phase at equilibrium	*ee* (%)
50:50	150	65.34	1200	1.31	1.31	97.38	S-D·2H_2O+R-D	86.66
50:50	150	65.34	1600	0.99	0.99	98.02	S-D·2H_2O	90.78
50:50	150	65.34	2000	0.79	0.79	98.41	S-D·2H_2O	91.52
50:50	150	65.34	2400	0.66	0.66	98.67	S-D·2H_2O	92.46
50:50	150	65.34	2800	0.57	0.57	98.86	S-D·2H_2O	95.80

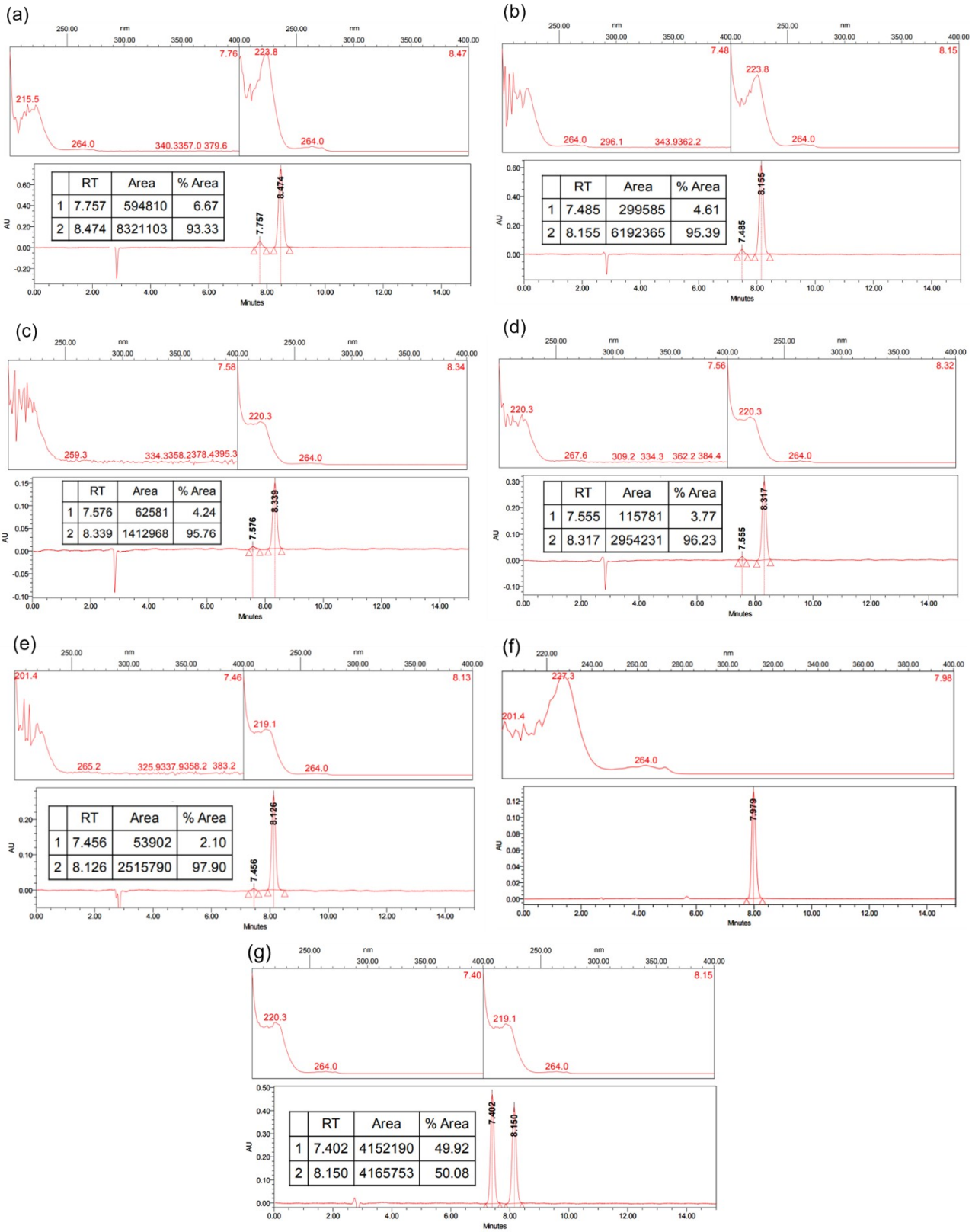

Fig. S14 Chiral HPLC results of the solid phases from five chiral resolution experiments, pure S-D·2H_2O and RS-IbuNa·2H_2O.

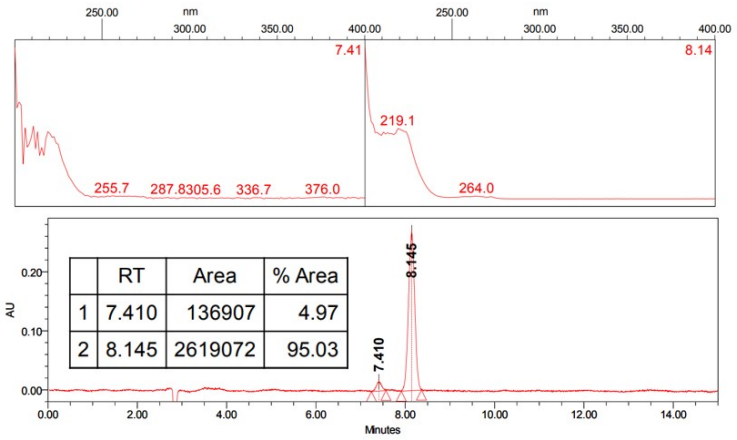

Fig. S15 Chiral HPLC result of the solid phase from the upscaled experiment.

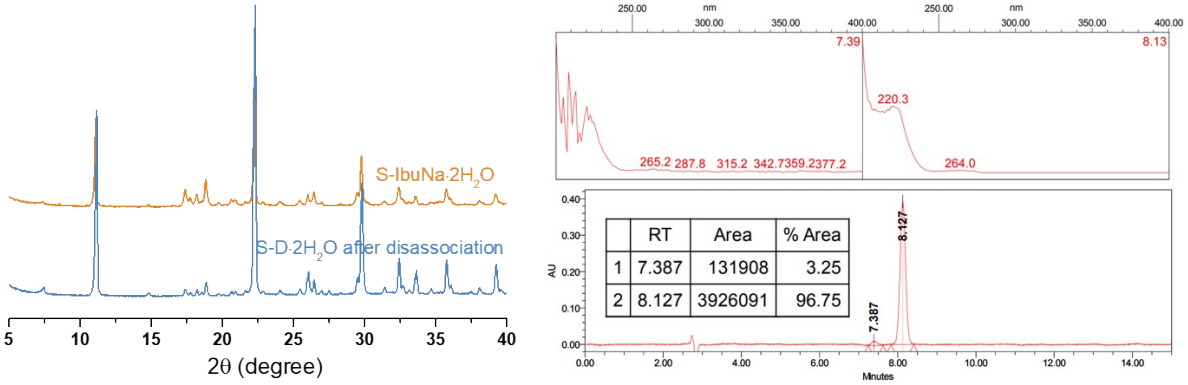

Fig. S16 PXRD and chiral HPLC result of the solid phase after dissociation experiment.

Table S7. Summary of reported chiral resolution results of RS-Ibuprofen using different methods.

Separation methods	Number of operations	*ee*
Diastereomer salt formation + supercritical fluid extraction[5]	1	<50%
Diastereomer salt formation + supercritical carbon dioxide[6]	1	<50%
Diastereomer salt formation + Couette-Taylor crystallizer[7]	1	<70%
Diastereomer salt formation[8]	2	72%
Diastereomer salt formation[9]	1	54%
Diastereomer cocrystal formation[10]	1	64%
Membrane separation[11]	1	17.8%
Membrane separation[12]	1	<25%
Membrane separation[13]	1	20.1%
Extraction[14]	1	50.4%

References

1 *CrysAlis^{Pro}*, version 1.171.37.35; Rigaku Oxford Diffraction.
2 G. M. Sheldrick, *Acta Crystallogr. A*, 2015, **71**, 3-8.
3 G. M. Sheldrick, *Acta Crystallogr. C*, 2015, **71**, 3-8.
4 O. A. Rahal, P. A. Williams, C. E. Hughes, B. M. Kariuki and K. D. Harris, *Cryst. Growth Des.*, 2021, **21**, 2498-2507.
5 P. Molnar, P. Bombicz, C. Varga, L. Bereczki, E. Szekely, G. Pokol, E. Fogassy and B. Simándi, *Chirality: The Pharmacological, Biological, and Chemical Consequences of Molecular Asymmetry*, 2009, **21**, 628-636.
6 G. Bánsághi, E. Székely, D. M. Sevillano, Z. Juvancz and B. Simándi, *J. Supercrit. Fluids*, 2012, **69**, 113-116.
7 L. Marc, S. Guillemer, J.-M. Schneider and G. Coquerel, *Chem. Eng. Res. Des.*, 2022, **178**, 95-110.
8 T. Q. Trung, J. M. Kim and K. H. Kim, *Arch. Pharmacal Res.*, 2006, **29**, 108-111.
9 H. L. Lee, Y. L. Hung, A. Amin, D. E. Pratama and T. Lee, *Ind. Eng. Chem. Res.*, 2023, **62**, 1946-1957.
10 B. Harmsen and T. Leyssens, *Cryst. Growth Des.*, 2018, **18**, 3654-3660.
11 X. Qiu, J. Ke, W. Chen, H. Liu, X. Bai, Y. Ji and J. Chen, *J. Membr. Sci.*, 2022, **660**, 120870.
12 W. R. Bowen and R. R. Nigmatullin, *Sep. Sci. Technol.*, 2002, **37**, 3227-3244.
13 N. Salehpour and S. Nojavan, *J. Membr. Sci.*, 2025, **717**, 123660.
14 G. Hu, Q. Lu, X. Mao, S. Qin, K. Yang and L. Ge, *Sustainable Chem. Pharm.*, 2025, **45**, 102009.